

Article

Quest for Compounds at the Verge of Charge Transfer Instabilities: The Case of Silver(II) Chloride [†]

Mariana Derzsi ^{1,2,*}, Adam Grzelak ¹, Paweł Kondratiuk ^{1,‡}, Kamil Tokár ^{2,3} and Wojciech Grochala ^{1,*}

¹ Center of New Technologies, University of Warsaw, Zwirki i Wigury 93, 02089 Warsaw, Poland

² Advanced Technologies Research Institute, Faculty of Materials Science and Technology in Trnava, Slovak University of Technology in Bratislava, 917 24 Trnava, Slovakia

³ Institute of Physics, Slovak Academy of Sciences, 845 11 Bratislava, Slovakia

* Correspondence: mariana.derzsi@gmail.com (M.D.); w.grochala@cent.uw.edu.pl (W.G.)

[†] This work is dedicated to the memory of Kazimierz Fajans (1887–1975).

[‡] Current Address: Institute of Theoretical Physics, Faculty of Physics, University of Warsaw, 02089 Warsaw, Poland.

Received: 5 July 2019; Accepted: 9 August 2019; Published: 15 August 2019



Abstract: Electron-transfer processes constitute one important limiting factor governing stability of solids. One classical case is that of CuI_2 , which has never been prepared at ambient pressure conditions due to feasibility of charge transfer between metal and nonmetal ($\text{CuI}_2 \rightarrow \text{CuI} + \frac{1}{2} \text{I}_2$). Sometimes, redox instabilities involve two metal centers, e.g., AgO is not an oxide of divalent silver but rather silver(I) dioxoargentate(III), $\text{Ag(I)[Ag(III)O}_2]$. Here, we look at the particularly interesting case of a hypothetical AgCl_2 where both types of redox instabilities operate simultaneously. Since standard redox potential of the Ag(II)/Ag(I) redox pair reaches some 2 V versus Normal Hydrogen Electrode (NHE), it might be expected that Ag(II) would oxidize Cl^- anion with great ease (standard redox potential of the $\frac{1}{2} \text{Cl}_2/\text{Cl}^-$ pair is + 1.36 V versus Normal Hydrogen Electrode). However, ionic Ag(II)Cl_2 benefits from long-distance electrostatic stabilization to a much larger degree than $\text{Ag(I)Cl} + \frac{1}{2} \text{Cl}_2$, which affects relative stability. Moreover, Ag(II) may disproportionate in its chloride, just like it does in an oxide; this is what AuCl_2 does, its formula corresponding in fact to $\text{Au(I)[Au(III)Cl}_4]$. Formation of polychloride substructure, as for organic derivatives of Cl_3^- anion, is yet another possibility. All that creates a very complicated potential energy surface with a few chemically distinct minima i.e., diverse polymorphic forms present. Here, results of our theoretical study for AgCl_2 will be presented including outcome of evolutionary algorithm structure prediction method, and the chemical identity of the most stable form will be uncovered together with its presumed magnetic properties. Contrary to previous rough estimates suggesting substantial instability of AgCl_2 , we find that AgCl_2 is only slightly metastable (by 52 meV per formula unit) with respect to the known AgCl and $\frac{1}{2} \text{Cl}_2$, stable with respect to elements, and simultaneously dynamically (i.e., phonon) stable. Thus, our results point out to conceivable existence of AgCl_2 which should be targeted via non-equilibrium approaches.

Keywords: silver; chlorine; learning algorithms; crystal structure; magnetic properties

1. Introduction

Electron-transfer processes constitute one important limiting factor governing stability of solids. One classic case is that of CuI_2 , which has never been prepared at ambient pressure conditions due to feasibility of charge transfer between metal and nonmetal. The energy of ligand-to-metal-charge

transfer (LMCT) is negative for CuI_2 which results in instability and phase separation, according to the Equation (1):



While the process of oxidation of iodide anions by Cu(II) is well-known to every chemistry freshman, it remains somewhat difficult to explain to a comprehensive school pupil, based on the values of standard redox potentials, E^0 , for the relevant species in aqueous solutions. The reason for that is that the E^0 value for the Cu(II)/Cu(I) redox pair is + 0.16 V versus NHE (Normal Hydrogen Electrode), while that for the $\text{I}_2/2 \text{I}^-$ is + 0.54 V, i.e., I_2 is formally a slightly better stronger oxidizer than Cu(II). The detailed explanation necessitates departure from the aqueous conditions (note, E^0 values are the feature of solvated species in aqueous solutions). Since Cu(II) in aqueous solutions is very strongly solvated by water molecules acting as a Lewis base ($\text{H}_2\text{O} \rightarrow \text{Cu(II)}$), and this effect surpassed the one of coordination of water molecules to Cu(I), the oxidizing properties of naked Cu(II) are certainly stronger than those of solvated ions. Simultaneously, since I^- anion is coordinated by water molecules acting like Lewis acid ($\text{OH}_2 \dots \text{I}^-$) (and coordination to anion is stronger than to neutral I_2 molecules) the E^0 value for the $\text{I}_2/2 \text{I}^-$ redox pair is actually larger than the one for unsolvated species. This helps to explain why the balance of a redox reaction for the phases in the solid state, i.e., lacking any solvent, is different from the one which might be guessed based on the plain E^0 values.

Attempts to more quantitatively explain the lack of stability of CuI_2 at ambient (p,T) conditions involve discussions of ionization potential of monovalent metal, ionic polarizabilities, as well as lattice energies of relevant solids. Over 60 years ago, following early considerations by Fajans [1], Morris estimated the standard molar free energy of formation of CuI_2 [2]. The obtained value was slightly positive, some 1 kcal/mole [2], see also [3]. Since the respective value for CuI is large and negative (circa -16.6 kcal/mole), it is natural that formation of CuI_2 is strongly disfavored. This, of course, may change under high pressure conditions, which—due to beneficial pV factor allowing to crowd cations and anions together in the lattice—often favor formation of species at high oxidation states.

Sometimes redox instabilities involve two metal centers rather than metal and nonmetal, e.g., AgO is not an oxide of divalent silver but rather silver(I) dioxoargentate(III), $\text{Ag(I)[Ag(III)O}_2]$ [4,5]:



The analogous behavior has been theoretically predicted for AuO, as well [6]. It is important to notice that the disproportionation reactions of this type are always energy uphill in the gas phase, and they are relatively rare for extended solids. In the case of silver, the energy of reaction proceeding according to Equation (2) is positive and very large, some 13.3 eV, as may be estimated from relevant ionization potentials (this value corresponds to the Mott-Hubbard U energy in the gas phase). The fact that the process takes place in AgO according to Equation (2) is given by several important factors, such as departure from ionic formulation, and the fact that U is strongly screened in solids. The rule of a thumb is that disproportionation processes are facile (i) in a Lewis-basic environment, (ii) especially when there is strong mixing of metal and nonmetal states i.e., pronounced covalence of chemical bonding, (iii) when the pV factor at elevated pressure, which prefers packing of unequal spheres, dominates the energetic terms, and (iv) at low temperatures [7]. AgO is in fact a nice exemplification of condition (i), since it is disproportionated, while its more Lewis acidic derivative, AgSO_4 , is not [8]. Another good example is that of $\text{Au(II)(SbF}_6)_2$, which is, comproporionated, a genuine Au(II) compound [9], while its parent basic fluoride, AuF_2 , has never been prepared in the solid phase, as it is subject to phase separation via disproportionation to Au and AuF_3 . Moreover, AgO exemplifies condition (ii), since the chemical bonding between Ag and O is remarkably covalent in this compound, which leads to a phonon-driven disproportionation [10]. Finally, AgO, also exemplifies condition (iii), since it remains disproportionated to a pressure of at least 1 mln atm [11].

Here, we look at the particularly interesting case of an elusive AgCl_2 where, as we will see, both types of redox instabilities may happen. Since the standard redox potential of the Ag(II)/Ag(I)

redox pair reaches some +2.0 V versus NHE and the respective value for the $\frac{1}{2}$ Cl₂/Cl[−] pair is +1.36 V, it might naturally be expected that Ag(II) would oxidize Cl[−] anion with great ease (the above-mentioned arguments valid for CuI₂ are also valid for AgCl₂). However, ionic Ag(II)Cl₂ benefits from long-distance electrostatic stabilization to a much larger degree than Ag(I)Cl + $\frac{1}{2}$ Cl₂, which should affect relative stability. Moreover, since the Ag(II)–Cl bonding is naturally expected to be quite covalent, similarly to the Ag(II)–O one in AgO (Cl and O have nearly identical electronegativities), Ag(II) might disproportionate in its chloride, just like it does in oxide. This is in fact what related AuCl₂ does, its true formula corresponding in fact to Au(I)[Au(III)Cl₄] [12]. Formation of polychloride substructure, as for organic derivatives of Cl₃[−] anion [13,14], or a mixed chloride-polychloride (Ag(I)₂(Cl)(Cl₃)), is yet another possibility. Last but not the least, AgCl₂ featuring an unpaired electron at the transition metal center may choose to form exotic Ag–Ag bond, as is observed for AuSO₄ [15]. All that creates a complicated potential energy surface with a few chemically distinct minima, i.e., diverse polymorphic forms present, and this renders theoretical predictions troublesome.

The major aim of this work is to theoretically predict crystal structure, stability, and presumed electronic and magnetic properties of the most stable form of AgCl₂. We would like also to computationally verify early predictions by Morris who estimated the free enthalpy of reaction:



to be strongly negative, some −96.4 kJ/mole [2]. Finally, we will briefly discuss the anticipated impact of elevated pressure on the course of the reaction described by Equation (3), as well as magnetic properties of the most stable phases found.

2. Methodology

This study has begun in resemblance with our previous theoretical search for AgSO₄, where we have employed the method of following imaginary phonon modes to reach dynamically stable structural models [16,17]. Using this method, we have optimized the hypothetical AgCl₂ crystal in all known crystal structure polytypes taken by metal dihalides, MX₂ (X = F, Cl, Br, I) (i.e., over 40 structure types) using the plane-wave code VASP (Vienna Ab-initio Simulation Package) [18–22], and subsequently calculated phonon dispersion curves for each model using the program PHONON [23]. In cases where at least one imaginary phonon was detected (signaling dynamic instability), we followed the normal coordinate of this mode to reach another, lower symmetry and lower energy structure [17,24], and we reexamined phonons after optimization. Due to complexity and CPU burden of the task this preliminary quest was conducted with LDA functional and lower plane-wave cut-off equal to 400 eV. In the second approach, the evolutionary algorithm approach was applied using XtalOpt [25–28] in combination with VASP and using GGA (general gradient approximation) with Perdew-Burke-Ernzerhof functional adapted for solids (PBEsol) and plane-wave cutoffs of 520 eV. Using the evolutionary algorithms, we have considered unit cells containing 2, 4, and 8 formula units and generated a pool of 2183 structures. The lowest energy structures originating from both methods were ultimately recalculated with spin-polarization, on-site Coulomb interactions and van der Waals corrections, as outlined below. Magnetic models were constructed for polymorphic forms containing genuine Ag(II) paramagnetic centers and the lowest energy spin arrangements were found using the rotationally invariant density functional theory DFT + U method introduced by Liechtenstein et al. where the values of both Hubbard U and the Hund J parameter are set explicitly [29]. The U and J parameters were set only for d orbitals of the Ag atoms and the values of 5 eV and 1 eV were used, respectively [30]. The van der Waals interactions were accounted for using the DFT-D3 correction method of Grimme et al. with Becke-Jonson damping [31]. Additionally, the hybrid DFT calculations with HSE06 functional were used to calculate the mixed-valence Ag^IAg^{III}Cl₂ solution that could not be properly stabilized at the DFT level.

Electronic density of states was calculated using the aforementioned DFT + U method with DFT-D3 van der Waals correction, with k-mesh of 0.025 \AA^{-1} and 800 eV plane-wave cutoff. The disproportionated AgCl_2 and AuCl_2 structures were additionally pre-optimized with HSE06 functional using a coarser k-mesh of 0.05 \AA^{-1} .

3. Results

3.1. Scrutiny of Dynamically Stable Polymorphic forms of AgCl_2 (Method of Following Imaginary Phonon Modes)

The crystal structures selected for preliminary study accounted for numerous polytypes known among the transition metal and alkali earth metal dihalides. Both more ionic as well as more covalent structural types were tested. AgF_2 , AuCl_2 , CuCl_2 , PdF_2 , PtCl_2 , PbCl_2 (cottunite), $\alpha\text{-PbO}_2$, and TiO_2 (rutile) were selected because of obvious structural analogies within Group 11 of the Periodic Table of Elements, or because they are often adopted by metal chlorides [24]. Among those, KAuF_4 and AuCl_2 types with K or Au atoms substituted by Ag ones, represent disproportionated Ag(I)/Ag(III) systems; others correspond to comproportionated ones. We have also employed a set of ionic halide structures, notably: CaF_2 (fluorite), CaCl_2 ($Pmn2_1$ and $Pnmm$ polytypes), CdCl_2 , layered CdI_2 , MgCl_2 ($P4m2$, $Ama2$ and $P-1$ polymorphs), SrI_2 , YbCl_2 , as well as polymeric BeF_2 , and three covalent structures: SiS_2 , FeP_2 , and XeF_2 . Altogether, these representative prototypes show a rich variety of structural motifs and lattice dimensionalities. Using the method of following the imaginary modes of AgCl_2 in these types of structures we have obtained over 10 dynamically stable structures. Figure 1a–f illustrates the six main structural motifs present in them. All remaining predicted polymorphs are simply various polytypes of these (differ in stacking of the main structural motifs).

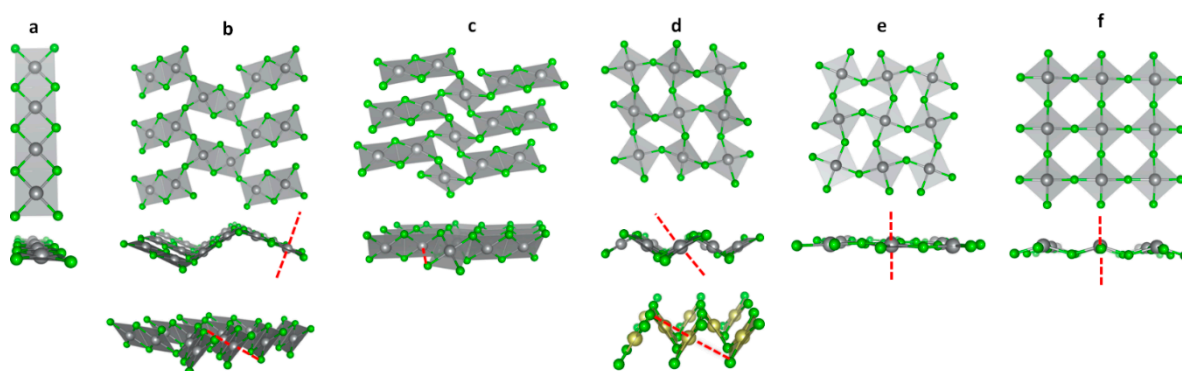


Figure 1. Illustration of main structural motifs that differ in connectivity of coordination polyhedra (the $[\text{AgCl}_4]$ plaquettes) for the dynamically stable polymorphs of a hypothetical AgCl_2 compound predicted using the method of following imaginary phonon modes. Top and side view is shown. In the side views, the axial Ag–Cl contacts that complete the octahedral coordination of silver atoms are indicated by red dotted line. In panel **b**, two side views represent two distinct polymorphs, respectively. The lower side view in panel **d** (bottom), represents highly puckered layer that is observed in some transition metal dihalides, but not in AgCl_2 (see text for further explanation). Color code: Ag—big grey balls, Cl—small green balls, Pd—big yellow balls.

The main structural building block in all dynamically stable models is a $[\text{AgCl}_4]$ plaquette. Here, silver is stabilized in a close to square-planar (or elongated octahedral) coordination by chloride anions, which is the most common coordination sphere of Ag^{II} cation among the known compounds [32]. Silver in the second oxidation state is seldom found in a linear (or a contracted octahedral) coordination, and other geometries are even more scarce. This behavior is nicely reflected by the results of our extensive structure screening. For example, the compressed octahedral coordination appeared in our search only once in a rutile type structure. Although predicted to be dynamically stable at DFT level, it was ruled out in the subsequent spin-polarized DFT + U calculations, where it converged to

a square-planar coordination. The 2 + 4 coordination is indeed more common for fluorides in rutile structure (PdF_2 and NiF_2), but no such chloride is known. In one case, a butterfly penta-coordination (i.e., close to a tetragonal pyramide) was obtained, where the silver atoms are displaced out of the plain formed by the $[\text{AgCl}_4]$ plaquettes (Figure 1f). Such geometry has been previously observed for Ag^{II} in two high-pressure polymorphs of AgF_2 : a layered and a tubular one [33]. In both, the silver atoms depart from the center of the ideally flat square-planar $[\text{AgF}_4]$ units to achieve better packing while simultaneously preserving the local Jahn–Teller distortion. The AgCl_2 structure with the butterfly silver coordination is topologically equivalent to the layered HP1 polymorph of AgF_2 . Indeed, it exhibits the lowest calculated volume among the predicted dynamically stable structures and thus it should be stabilized at high pressure (see section 3). Our scrutiny of AgCl_2 polytypes provides theoretical evidence that the butterfly coordination is indeed a natural response of octahedral Ag^{II} sites (4 + 2 coordination) to high pressures and it permits more effective packing of 4 + 1 + 1 distorted $[\text{Ag}^{\text{II}}\text{X}_6]$ units.

The $[\text{Ag}^{\text{II}}\text{X}_4]$ squares show three distinct connectivity patterns in the dynamically stable polymorphs. They are connected either by corners, edges or via a combination of the two, while the resulting lattice is one- or two-dimensional at most. This comes as no surprise since it is natural for the strongly Jahn-Teller active cation to exhibit reduced structural dimensionality in its compounds. Here, the edge sharing always results in one-dimensional chains that have a shape of infinite molecular ribbons (Figure 1a). On the other hand, corner and combined corner plus edge sharing leads always to layered structures (Figure 1b–f). No polymorphs with isolated $[\text{AgCl}_4]$ units or three-dimensional connectivity were found. Additionally, it may be noticed that each chlorine atom is always shared between two Ag cations thus AgCl_2 strictly avoids chlorine terminals in its structures. This, too, is quite natural, since Ag^{II} is an electron deficient and Lewis acidic cation, which attempts to satisfy its need for electronic density by having at least four anions in its coordination sphere; at AgCl_2 stoichiometry this implies ligand sharing, i.e., $[\text{AgCl}_{4/2}]$. The charge depletion on Cl atoms affects the halogen-halogen interactions, as discussed in Supplementary Materials (S1).

Structures with infinite ribbons are characteristic of dihalides containing Jahn-Teller active cations and are also present in cuprates such as LiCu_2O_2 [34] and LiCuVO_4 [35]. In halides, the ribbons have neutral charge and these structures are held together by van der Waals interactions. In the cuprates, the ribbons are present as anionic species $[\text{CuO}_2]^{2-\infty}$, whose charge is compensated by the presence of additional metal cations. Although observed in majority of halides containing Jahn-Teller ions including CuCl_2 , CuBr_2 , PdCl_2 , PtCl_2 , and CrCl_2 , they have never been observed in compounds of silver. Importantly, for AgCl_2 this structure polytype has the lowest computed energy as will be discussed later in the text.

Three distinct structural patterns are observed among the layered polymorphs. In the first case, fragments of the ribbons may be distinguished that consist of two $[\text{AgCl}_4]$ units sharing one edge. These $[\text{Ag}_2\text{Cl}_6]$ dimers then interconnect into layers by sharing corners (Figure 1b). Another structural pattern is formed by alternation of the same dimers with single squares (Figure 1c). The third type of layers is formed by squares sharing only corners (Figure 1d–f). The layered polymorphs containing the dimeric units are unique among the halides. They are closely related to orthorhombic ramsdellite [36] and monoclinic $\gamma\text{-MnO}_2$ polymorph form [37]. The ramsdellite structure consists of three-dimensional network of double chains of edge-sharing MnO_6 octahedra while in the $\gamma\text{-MnO}_2$ the double chains alternate with single chains of MnO_6 octahedra (Figure 2a,b). In the predicted AgCl_2 polymorphs with the dimeric $[\text{Ag}_2\text{Cl}_6]$ units (Figure 1b), the three-dimensional network of the ramsdellite structure is reduced to two-dimensional one due to Jahn-Teller distortion of the octahedra that takes place in the direction parallel to the propagation of the chains. The same relation exists between the AgCl_2 polymorph formed by alternation of the $[\text{Ag}_2\text{Cl}_6]$ dimers with $[\text{AgCl}_4]$ squares (figure 1c) and the $\gamma\text{-MnO}_2$ structure. Although no such halides exist, the ramsdellite-related AgCl_2 structure has its zero-dimensional analogues in 4d and 5d transition metal pentachlorides such as MoCl_5 , $\text{Ta}_2\text{Cl}_{10}$, NbCl_5 , WCl_5 . They consist of dimeric M_2Cl_{10} units of edge-sharing MCl_6 octahedra

ordering patterns and thus various types of connectivity of the $[\text{AgCl}_4]$ plaquettes. While the same orientation of the d_{z^2} orbitals along the A direction (ferrodistortive AAA orbital ordering pattern) leads to the ribbon polymorphs, alternating orientation of the orbitals (antiferrodistortive ordering patterns) results in layered polymorphs featuring corner-shared $[\text{Ag}_2\text{Cl}_6]$ dimers. Here, the Jahn-Teller distortion takes place alternatively along the B and C direction while two such orbital ordering patterns are possible. The AACAAC orbital ordering pattern leads to a layer containing monomeric and dimeric units (Figures 1c and 3d) and AACC pattern to a layer containing only dimeric units (Figures 1b and 3e).

CdI_2 structure allows also for derivation of the layers with corner-sharing plaquettes, which may be achieved by ACAC ordering pattern and is in fact observed in low-temperature $\gamma\text{-PdCl}_2$ (Figure 1d, bottom) [38]. However, the predicted layered polymorphs of AgCl_2 with corner-sharing no longer belong to the CdI_2 family but rather to rutile and fluorite family as manifested by change of the axial coordination of the Ag atoms from intralayer to interlayer one (Figure 1d–e). Note that in all the ribbon and layered polymorphs derived from the CdI_2 structure, the cations are always octahedrally coordinated by intralayer anions; that is, by anions belonging to the same CdI_2 -type layer. On the other hand, the silver atoms from the corner-shared AgCl_2 layers complete their octahedral coordination by axial chlorine atoms from adjacent layers (Figure 1). To do so, the CdI_2 layers must become less corrugated. Such geometrical arrangements are characteristic of a rutile structure. This prototypical structure consists of three-dimensional network of corner- and edge-shared octahedra. Orbital ordering at Jahn-Teller active cations in these octahedra may result in formation of layers consisting of corner-shared plaquettes, where each metal cation from each plaquette is axially coordinated by anions from adjacent layers, as exemplified by CuF_2 structure (Figure 4b). Furthermore, various stacking patterns of these layers may be realized. The simplest AA stacking is stabilized in the monoclinic CuF_2 type and the ABAB stacking in the orthorhombic AgF_2 type. Yet another structure with $\text{AB}'\text{AB}'$ stacking was found that differs from the AgF_2 type by smaller relative shift of the layers (an intermediate between CuF_2 and AgF_2 structure) (Figure 5). These various stacking patterns result in different axial contacts of the cations and diverse packing efficiencies. Recall that CuF_2 is rutile type structure. On the other hand, the AgF_2 structure is related to fluorite structure, where the cations reach for two additional ligands to complete a cubic coordination [11]. Compounds with rutile-like structures often transform to denser fluorite-like structure under pressure. Thus, three distinct stable layered forms of AgCl_2 - CuF_2 type, AgF_2 type, and intermediate between the two with different stacking of the layers, might be achieved under different pressure conditions. More on that later.

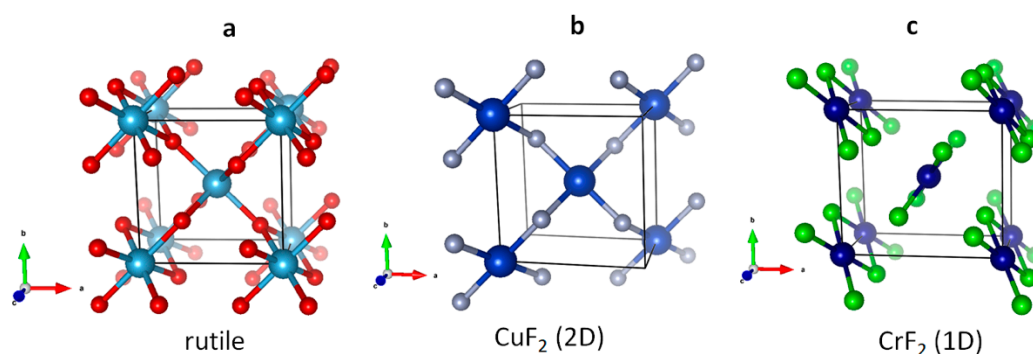


Figure 4. Crystal structure of rutile highlighting the edge- and corner-shared octahedra (a), rutile-derived two-dimensional (2D) CuF_2 - (b) and a hypothetical one-dimensional (1D) ribbon structure (c) achieved by octahedral elongation along two distinct octahedral directions.

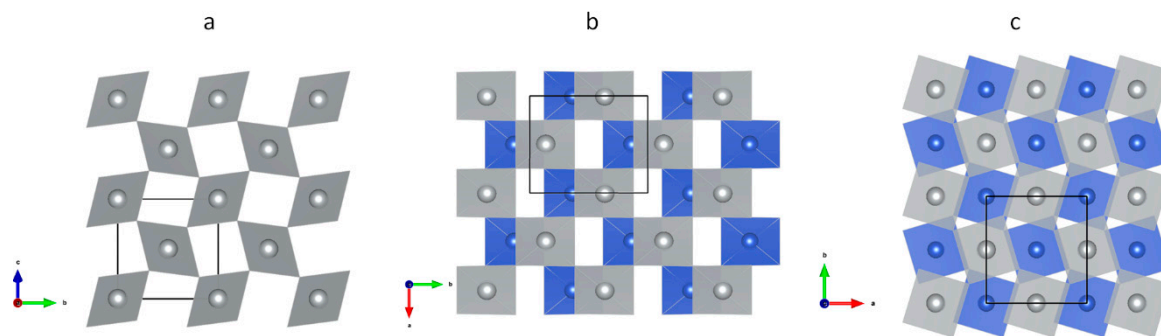


Figure 5. Three stacking patterns realized in the predicted layered AgCl_2 polymorphs with corner-sharing of $[\text{AgCl}_4]$ plaquettes: AA stacking of rutile-related CuF_2 type (a), AB' stacking (b), and AB stacking of fluorite-related AgF_2 type (c). The $[\text{AgCl}_4]$ plaquettes belonging to different layers are distinguished by different color (blue and grey).

Similarly, as in the case of the layered structures, several polytypes were found for the ribbon structures. While the AgCl_2 ribbons maintain the layered organization of the CdI_2 prototype with the interlayer contacts being longer than the intralayer ones, stacking of these layers may vary (Figure 6). We have obtained various polytypes in our search using evolutionary algorithms. The simplest stacking corresponds to one layer per unit cell that directly relates to the CdI_2 type structure. The original trigonal $P-3m$ symmetry of the CdI_2 type is however lowered to triclinic due to the presence of the Jahn-Teller active Ag^{II} cation. Additionally, a monoclinic $C2m$ structure of copper dihalide type was found in our scrutiny, as well as an orthorhombic and a triclinic version of the PdCl_2 polymorphs (Figure 6). Note, PdCl_2 crystallizes in two ribbon-like structures, a high-temperature orthorhombic and a low-temperature monoclinic form, which differ only in the monoclinic angle. Our results provide theoretical support for the observed strong tendency of the late TM dihalides with Jahn-Teller cations to form ribbon-like crystal structures exhibiting various packing.

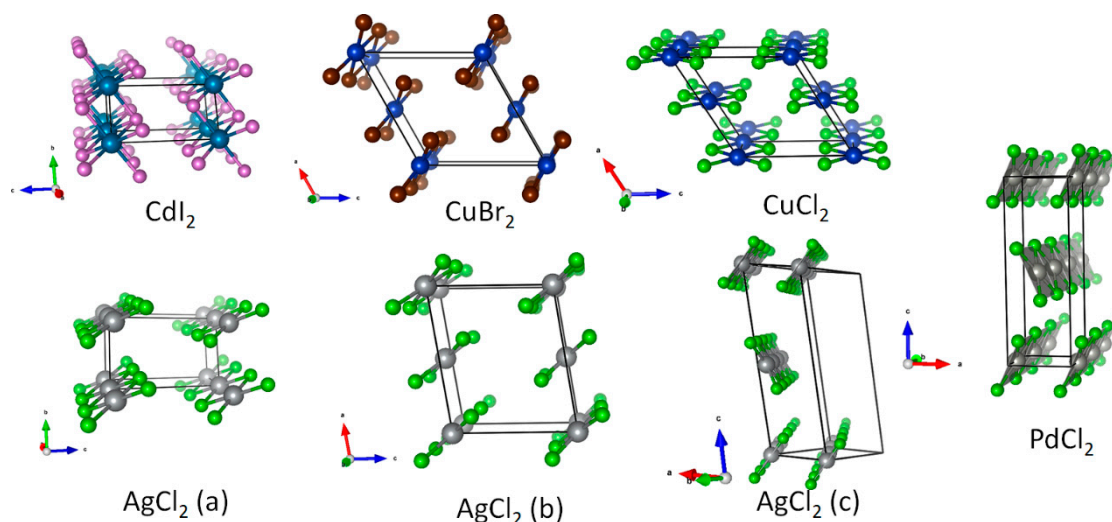


Figure 6. Three hypothetical AgCl_2 ribbon-like polytypes (bottom) obtained with evolutionary algorithms and their relation to the CdI_2 prototype (top left) and the known metal halides with ribbon structure (top and right). The differences of computed energy for (a–c) are minuscule.

Note that both rutile and fluorite structures are prototype structures for ionic crystals, while the CdI_2 structure is preferred by compounds forming more covalent bonds. In the predicted polymorphs of AgCl_2 , we see frequent realization of structures related to both more ionic as well as more covalent structural types. This may be a manifestation of the intermediate character of the chemical bonding in AgCl_2 .

3.2. The Unusual $\text{Ag(I)Cl}(\text{Cl}_2)_{\frac{1}{2}}$ Polymorph

As explained in the introduction, one of the key difficulties in preparation of the Ag(II) dichloride from elements or from AgCl and excess of Cl_2 is related to the fact that Ag(II) is a potent oxidizer. This means that silver might prefer to adopt its most common monovalent state (as AgCl), while the excess Cl atom would be forced to form Cl–Cl bonds with other similar species around. On the other hand, the so-formed Cl_2 is known to interact with Cl^- anions in ionic compounds, by forming an asymmetric $[\text{Cl}^- \dots \text{Cl}_2]$ or even symmetric $[\text{Cl}-\text{Cl}-\text{Cl}^-]$ [39–41] trichloride anion. While the propensity of Cl_3^- to form is much smaller than that of the related triiodide anion, yet such a Lewis structure should not escape our attention. Indeed, the XTalOpt quest has yielded one structure with the $\text{Ag(I)Cl}(\text{Cl}_2)_{\frac{1}{2}}$ formulation (Figure 7). It consists of AgCl double layers with Cl_2 molecules sandwiched in between them.

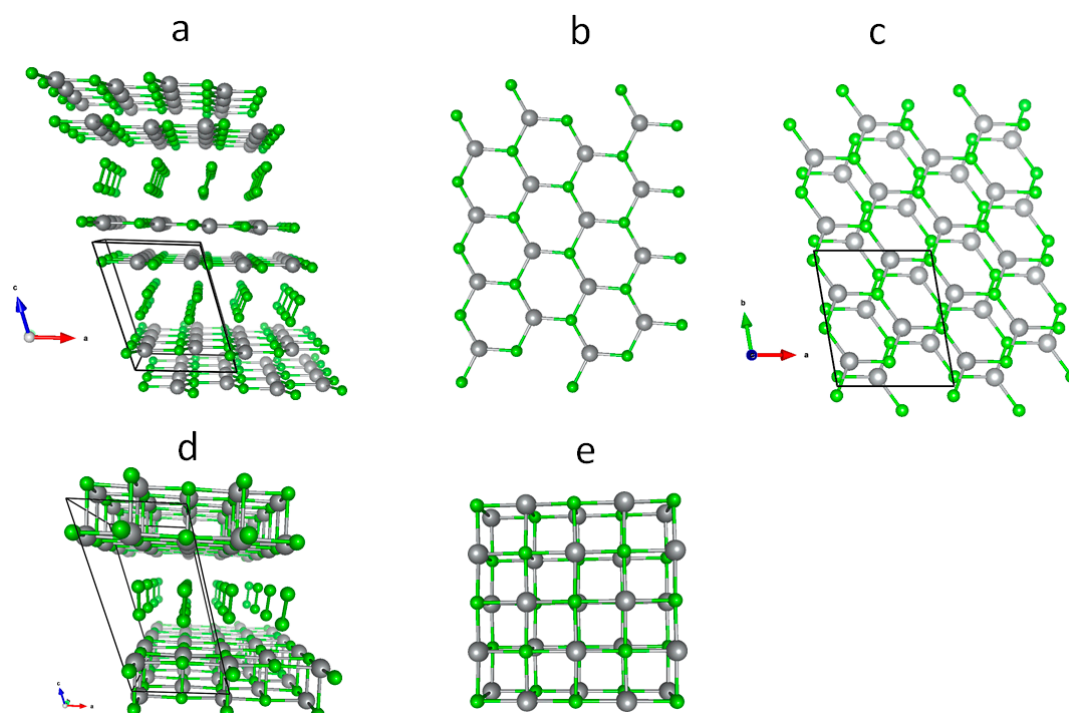


Figure 7. The predicted $\text{Ag(I)Cl}(\text{Cl}_2)_{\frac{1}{2}}$ polymorphs: the crystal structure with hexagonal AgCl_2 double layers highlighting the unit cell, one AgCl layer and stacking of the AgCl layers, respectively (a–c), and an alternative structure with rock-salt AgCl double layers (d,e).

The structures of $\text{Ag(I)Cl}(\text{Cl}_2)_{\frac{1}{2}}$ consist of the AgCl layers which can form either rock-salt layers or pseudo-hexagonal ones with only three short Ag–Cl bonds (Figure 7). The appearance of the rock salt layers seems natural since AgCl in rock salt structure is well known. However, the hexagonal layers are unknown among plain Ag(I) halides, with AgX ($X = \text{F}, \text{Cl}, \text{Br}, \text{I}$) adopting an ionic NaCl polytype (CN = 6), while AgI additionally takes on several structures with tetrahedral coordination of cation (CN = 4) (i.e., wurtzite, sphalerite, SiC(4H), etc.). In addition, CN of 7 is also possible for AgCl at rather low pressure of circa 1 GPa (TiI polytype [42]). The very low CN of 3 for Ag(I) in pseudo-hexagonal BN-like layer and a very short bond length of 2.521 Å indicates more covalent in respect the rock salt structure (six bonds at 2.773 Å [42]). Since the intra-sheet Ag–Cl bonding is covalent, it is not surprising to see that the interactions of Cl_2 with Cl^- anions are far from symmetric, with intra-molecular Cl–Cl bond of 2.054 Å (slightly longer than that found for molecular solid of Cl_2 , 1.97 Å), and $\text{Cl} \dots \text{Cl}^-$ separation of 2.874 Å. That the Cl–Cl bond length is slightly longer than for free Cl_2 obviously stems from the donor-acceptor character of the $\text{Cl}^- \dots \text{Cl}_2$ interactions, and slight occupation of the σ^* orbital of Cl_2 .

Formation of AgCl intercalated with Cl₂ molecules is peculiar given substantial lattice energy of AgCl solid, and little energy penalty to break weak Cl[−] ... Cl₂ interactions upon phase separation to AgCl and $\frac{1}{2}$ Cl₂. Their appearance in our quest is probably related to the limit imposed to Xtalopt on number of formula units and it marks the tendency towards the phase separation. We will turn to stability of these structures in the next section and discuss pressure effects further on.

3.3. Relative and Absolute Energetic and Thermodynamic Stability of Several Important Polymorphic Forms of AgCl₂

The crystal structures of all polymorphs considered here has been provided as cif files in Supplementary Materials (S2).

At DFT + U + vdW level the edge-sharing connectivity that leads to infinite AgCl₂ stripes (Figure 1e) was found to be the most energy preferred one among the Ag(II)Cl₂ polymorphs. All ribbon polytypes are maximally 5 meV/FU apart in energy. Among the layered structures, the most preferred is the ramsdellite related structure, then the γ -MnO₂ related (Figure 1b,c and Figure 2a,b) and finally the CuF₂ and AgF₂ related structures. The ramsdellite related structure (monoclinic space group) is only circa 40 meV/FU higher in energy than the ribbon polymorphs (Table 1). This energy order reflects preference of Ag(II)Cl₂ for edge connectivity of the [Ag(II)Cl₄] square-planar units. Notably, all ribbon and puckered layered polymorphs are maximally 60 meV/FU apart. There is a considerable energy gap of about 200 meV/FU between the structures with puckered and flat layers; this is a manifestation of the fact that Ag(II)-Cl[−] bonding is markedly covalent and it is characterized by close-to sp² hybridization at Cl atoms, which in turn comes with bending of the Ag-Cl-Ag angles. Concerning the structures containing Ag(I), the unusual Ag(I)[Cl(Cl₂) $\frac{1}{2}$] form with rock salt AgCl double layers is preferred over the one with hexagonal layers by 136 meV/FU. Furthermore, it represents the overall global minimum. The zero-point energy further plays in favor of this structure, by additional 10meV/FU. Within the DFT + U picture, all predicted AgCl₂ polymorphs have negative formation energies and are thus energetically preferred over the elemental silver and molecular chlorine. However, they are metastable with respect to AgCl crystal. Calculated DFT + U energies of the lowest energy AgCl₂ forms are listed in Table 1 along with AgCl, molecular chlorine in its high-temperature polymorphic form [43], and elemental silver.

Table 1. Calculated DFT + U volumes and energies including van der Waals correction (E), zero-point energies (ZPE) and formation energies calculated in respect to the elemental crystals ($E^1_{\text{form}} = E - E_{\text{Ag} + \text{Cl}_2}$) as well as to AgCl and $\frac{1}{2}$ Cl₂ ($E^2_{\text{form}} = E - E_{\text{AgCl} + \frac{1}{2}\text{Cl}_2}$) for five prototypical AgCl₂ polymorphs. The formation energies are calculated considering high-temperature crystal structure of Cl₂ [43]. Volume values in brackets come from experiment. The formation energy for AgCl is calculated as $E_{\text{form}} = E - E_{\text{Ag} + \frac{1}{2}\text{Cl}_2}$. FU = formula unit.

Phase	Z	V/FU (Å ³)	E (eV/FU)	$E^1_{\text{form}}/\text{FU}$ (eV)	$E^2_{\text{form}}/\text{FU}$ (eV)	ZPE/FU (eV)	$V_{\text{form}}/\text{FU}$ (Å ³)
Ribbon AgCl ₂ (CdI ₂ related)	4	65.7	-7.683	-0.840	+0.136	0.080	+3.6
Layered AgCl ₂ (ramsdellite related)	4	66.7	-7.643	-0.800	+0.176	0.077	+4.6
Layered AgF ₂ type	4	63.0	-7.625	-0.782	+0.194	0.081	+0.9
Ag(I)[Cl(Cl ₂) $\frac{1}{2}$] (rocksalt AgCl layers)	8	65.0	-7.718	-0.875	+0.101	0.070	+2.9
Ag(I)[Cl(Cl ₂) $\frac{1}{2}$] (hex AgCl layers)	8	77.2 *	-7.582	-0.739	+0.237	0.069	+15.1 *
AgCl + $\frac{1}{2}$ Cl ₂		62.1	-7.819			0.027	
Cl ₂	4	47.6 (58.1)	-4.288			0.029	
AgCl	4	38.3 (42.7)	-5.675	-0.976		0.021	-1.0
Ag fcc	4	15.5 (17.1)	-2.555			0.012	

* The unusually large calculated volume of this phase clearly suggests that it originates from attempts of XtalOpt to separate Cl₂ and AgCl phases, hence this phase may not correspond to any real local minimum, i.e., it may not be observable.

Inspection of the calculated energies and volumes of various phases of the AgCl₂ stoichiometry (Table 1) reveals that:

1. While all forms of AgCl_2 are stable with respect to elements, none of AgCl_2 polymorphs is energetically stable at $T \rightarrow 0$ K and $p \rightarrow 0$ atm with respect to products from Equation (3), i.e., AgCl and $\frac{1}{2} \text{Cl}_2$.
2. The (relatively) most stable phase is that of $\text{Ag(I)[Cl(Cl}_2\text{)}_{\frac{1}{2}}]$ (rocksalt AgCl layers), as it falls at circa 0.1 eV above $\text{AgCl} + \frac{1}{2} \text{Cl}_2$.
3. The ZPE correction changes very little the relative ranking of structures (it varies by no more than 12 meV for various phases), and for absolute stability of phases with respect to products (it destabilizes them by additional circa 42–53 meV), as could be expected for the system composed of rather heavy elements, Ag and Cl.

We have recalculated the total electronic energies and volumes of selected polymorphs also on much more resources-consuming hybrid DFT level using HSE06 functional (Table 2). Guided by the previous result, we did not perform daunting ZPE calculations this time.

Table 2. Calculated HSE06 volumes and energies and formation energies calculated with respect to the elemental crystals ($E^1_{\text{form}} = E - E_{\text{Ag} + \text{Cl}_2}$) as well as to AgCl and $\frac{1}{2} \text{Cl}_2$ ($E^2_{\text{form}} = E - E_{\text{AgCl} + \frac{1}{2} \text{Cl}_2}$) for five prototypical AgCl_2 polymorphs. The formation energies are calculated considering high-temperature crystal structure of Cl_2 [43]. Volume values in brackets come from experiment. The formation energy for AgCl is calculated as $E_{\text{form}} = E - E_{\text{Ag} + \frac{1}{2} \text{Cl}_2}$.

Phase	Z	V/FU (\AA^3)	E (eV/FU)	$E^1_{\text{form}}/\text{FU}$ (eV)	$E^2_{\text{form}}/\text{FU}$ (eV)	ZPE/FU (eV)	$V_{\text{form}}/\text{FU}$ (\AA^3)
Ribbon AgCl_2 (CdI_2 related)	4	77.6	−9.848	−1.030	+0.052	ND	+8.1
Layered AgF_2 type	4	68.7	−9.727	−0.909	+0.173	ND	−0.8
$\text{Ag(I)[Cl(Cl}_2\text{)}_{\frac{1}{2}}]$ (rocksalt AgCl layers)	8	70.7	−9.839	−1.021	+0.061	ND	+1.2
$\text{Ag(I)[Cl(Cl}_2\text{)}_{\frac{1}{2}}]$ (hex AgCl layers)	8	83.9 *	−9.837	−1.019	+0.063	ND	+14.4 *
AuCl_2 -type (disproportionated)	4	76.9	−9.736	−0.918	+0.164	ND	+8.2
$\text{AgCl} + \frac{1}{2} \text{Cl}_2$		69.5	−9.900			ND	
Cl_2	4	56.8 (58.1)	−5.536			ND	
AgCl	4	41.1 (42.7)	−7.132	−1.082		ND	−4.2
Ag fcc	4	16.9 (17.1)	−3.282			ND	

* The unusually large calculated volume of this phase clearly suggests that it originates from attempts of XtalOpt to separate Cl_2 and AgCl phases, hence this phase may not correspond to any real local minimum, i.e., not be observable.

The hybrid DFT results for AgCl_2 (Table 2) show that:

1. While all forms of AgCl_2 are stable with respect to elements, none of AgCl_2 polymorphs is energetically stable at $T \rightarrow 0$ K and $p \rightarrow 0$ atm with respect to products from Equation (3), i.e., AgCl and $\frac{1}{2} \text{Cl}_2$; thus, confirming the DFT + U + vdW (van der Waals correction) results.
2. The (relatively) most stable phase is that of ribbon Ag(II)Cl_2 form as it falls at a mere 52 meV above $\text{AgCl} + \frac{1}{2} \text{Cl}_2$.
3. HSE06 calculations predict the unit cell volumes of Ag, Cl_2 , and AgCl quite well. The large calculated volume of the ribbon polymorph should be taken with a grain of salt, and this structure is bound only by weak vdW inter-ribbon interactions. The layered AgF_2 -type structure is the only one for which the formation reaction volume is slightly negative.

Here, the unusual $\text{Ag(I)[Cl(Cl}_2\text{)}_{\frac{1}{2}}]$ form with hexagonal AgCl double layers and its rock salt layer analogue were found to be energetically almost degenerate within 2 meV/FU. The unusual $\text{Ag(I)[Cl(Cl}_2\text{)}_{\frac{1}{2}}]$ form with hexagonal layers was found to be only 11 meV/FU higher in energy in respect to the ribbon polymorph. Recall that the ZPE of the $\text{Ag(I)[Cl(Cl}_2\text{)}_{\frac{1}{2}}]$ forms is by circa 10–11 eV/FU lower with respect to the ribbon polymorph (Table 1), which points to factual energy degeneracy of all three solutions considering the hybrid DFT free energies and DFT + U ZPE energies.

Hybrid DFT was also used to model mixed valence (i.e., charge density wave) Ag(I)Ag(III)Cl_4 solution, which could not be captured properly on DFT + U level. We have chosen for this purpose crystal structure of AuCl_2 , which forms molecular crystal with weakly bonded $\text{Au(I)}_2\text{Au(III)}_2\text{Cl}_8$

units [12]. Ag(III) cations are here in square planar $[\text{AuCl}_4]$ coordination and Au(I) in linear $[\text{AuCl}_2]$ coordination. These molecular units are stacked along one direction along which they polymerize into infinite chains under $\text{Au} \rightarrow \text{Ag}$ substitution. In the polymerized chains, the Ag(III) cations retain the square-planar coordination, while the Ag(I) cations pick up third chlorine ligand to form triangular instead of linear coordination. The triangular coordination is a consequence of Ag(I) moving closer to a chlorine atom belonging to the Ag(III) from the neighboring Ag(I)Ag(III)Cl_2 molecular unit. The Ag(I)-Cl bonds are then obviously longer (2.5 Å) in comparison to the Au(I)-Cl ones (2.3 Å) in the original AuCl_2 structure. On DFT + U level, the model converges to the one featuring chains of the comproportionated cations ($\text{Ag}^{\text{I}}\text{Ag}^{\text{III}} \rightarrow \text{Ag}^{\text{II}}\text{Ag}^{\text{II}}$). This comproportionation is structurally manifested by Ag(I) cation picking up a fourth chlorine atom with which it completes square planar coordination of newly formed Ag(II) cation (the newly created Ag-Cl bond is highlighted by red dashed line in Figure 8b, bottom). Such polymerized Ag(II)Cl_2 chains are isostructural with recently discovered tubular form of AgF_2 that forms under high pressure (Figure 8c,d) [11]. In AgCl_2 , the mixed valence chains are slightly energetically preferred (by circa 10 meV/FU) over the comproportionated ones at the hybrid DFT level. However, both are 100 meV/FU higher in energy with respect to the lowest energy ribbon polymorph.

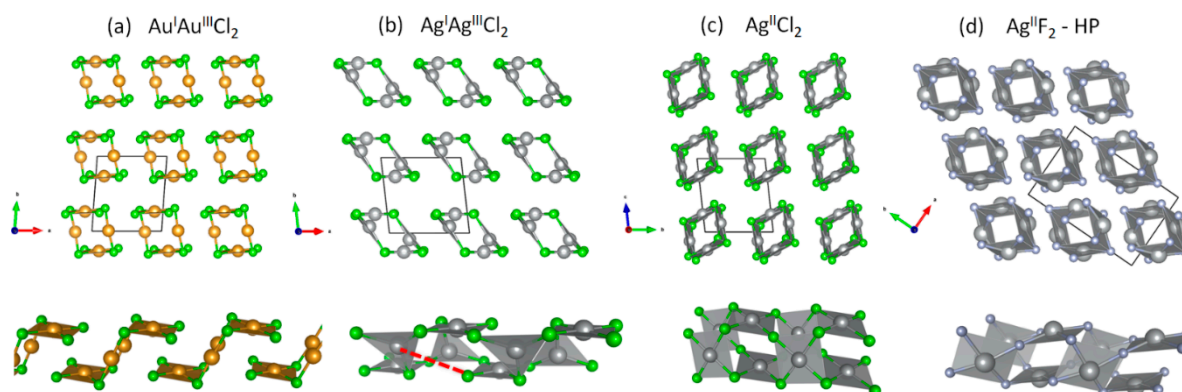


Figure 8. Crystal structure of Au(I)Au(III) Cl_4 (a), AgCl_2 optimized in the Au(I)Au(III) Cl_4 structure (b), AgCl_2 optimized in the Au(I)Au(III) Cl_4 structure with the symmetry-enforced comproportionation $\text{Ag}^{\text{I}}\text{Ag}^{\text{III}} \rightarrow \text{Ag}^{\text{II}}\text{Ag}^{\text{II}}$ (c) and high-pressure polymorph of AgF_2 (d). Top view: stacking of the chains, bottom view: connectivity within single chain.

3.4. Impact of Temperature and Pressure on Stability and Polymorphism of AgCl_2

Due to very similar energies of different polymorphs of AgCl_2 at $T \rightarrow 0$ K and $p \rightarrow 0$ GPa (also at the HSE06 level), and relatively small energy favouring the products of Equation (3) (AgCl and $\frac{1}{2} \text{Cl}_2$), stability and polymorphism of AgCl_2 are expected to be dependent on (p, T) conditions. Here, we look briefly at the impact of external parameters on stability of AgCl_2 .

The influence of temperature on stability of AgCl_2 is expected to be small in the range where Cl_2 is solid or liquid (i.e., up to its boiling point of -34 °C); the large reaction volume for the ribbon polymorph (Table 2), which is overestimated anyway, is insufficient to stabilize this phase via entropy factor [44]. Further increase of temperature will lead to preference for $\text{AgCl} + \frac{1}{2} \text{Cl}_2$ via the entropy (ST) factor of the Cl_2 gas. The ST factor for $\frac{1}{2} \text{Cl}_2$ at 300 K equals 347 meV [45] and thus, assuming that most of reaction volume change corresponds to the volume of Cl_2 gas released, it may be estimated that ΔG^0 of AgCl_2 formation is about + 0.4 eV at 300 K. While this is only 40% of what Morris predicted (i.e., circa 1 eV) [2], the value is still substantial. Our results point out at the lack of thermodynamic stability of AgCl_2 at any temperature conditions (in the absence of external pressure effects).

The situation is somewhat different when the impact of external pressure is considered. Here, the infinite-sheet AgF_2 -like form could potentially be stabilized at elevated pressure, as its formation from solid AgCl and $\frac{1}{2} \text{Cl}_2$ is accompanied by small volume drop. The common tangent method [17,46] allows for a rather crude estimate for the formation pressure of AgCl_2 of 35 GPa (at $T \rightarrow 0$ K), and likely

even higher pressures at elevated temperature. The more precise estimate requires calculations in the function of pressure to be performed, also including the ribbon polymorph, which should exhibit substantial compressibility, and several viable high-pressure polymorphs [11,47,48]. Moreover, while drawing the computed volume-based conclusions one should always remember that despite great performance of HSE06 functional for describing crystal and electronic structure of solids, the reproduction of van der Waals interactions is still imperfect. And since they tend to collapse fast under even moderate pressures, it could be that other polymorphic forms, such as the ribbon one, would become competitive at rather low pressures, even preceding the transformation to the layered form. The previously documented pressure-induced transformations of CuF_2 [47] and AgF_2 [11] as well as a large body of data for transition metal difluorides and dichlorides (see also [48] and references therein) seem to suggest this scenario as a viable one.

3.5. Magnetic Properties of Selected Polymorphic Forms of AgCl_2

If chemistry teaches us something important, it is that virtually any chemical composition may be studied in its metastable form, given that the local minimum is protected by sizeable energy and/or entropy barriers. Thus, while AgCl_2 may not be thermodynamically stable at a broad range of (p,T) conditions, it is still insightful to theoretically study selected properties of AgCl_2 , and compare them to those of the related halides (CuCl_2 , AgF_2 , AuCl_2 , etc.).

For all Ag(II)Cl_2 forms featuring paramagnetic silver, the magnetic ordering is of interest, especially that magnetic properties of Ag(II) fluorides are now under intense scrutiny [49,50]. Thus, we have looked at spin ordering patterns, spin exchange pathways, as well as relevant superexchange constants for the ribbon and layered polymorphs of AgCl_2 (Table 3).

Table 3. Calculated energies, relative energies, and magnetic moments on atoms for the ribbon and AgF_2 -type model of AgCl_2 as calculated using DFT + U + vdW. The unit cell was optimized for the ground state model (AFM1 in a ribbon and AFM in AgF_2 -type structure), while energies of the remaining magnetic models were calculated as single point energies from the ground state.

Form	Ordering Pattern	E/FU (eV)	E_rel/FU (meV)	Ag (m_B)	Cl(m_B)
Ribbon polymorph	AFM1 (AABB)	-7.683	0	± 0.31	± 0.21 for F joining two like Ag spins ± 0.00 between opposite Ag spins
	AFM2 (ABAB)	-7.652	31	± 0.31	± 0.10 on all F
	FM (AAAA)	-7.640	43	+0.35	+0.26 on all F
AgF_2 -type	AFM	-7.625	0	± 0.24	± 0.10
	FM	-7.549	76	+0.35	+0.26

Not surprisingly, in the case of the ribbon polymorph the magnetic ground state found here is identical to that exhibited by structurally related frustrated Heisenberg chain system, CuCl_2 , i.e., the spin pattern is AABB [51]. Correspondingly, as for CuCl_2 we consider the next neighbor (J_1) as well as the next near neighbor (J_2) superexchange constants (Figure 9), while neglecting all weaker magnetic interactions [51]. From the equations relating the energies of AFM1, AFM2, and FM states, and using the same Hamiltonian as authors [51]:

$$E_{\text{AFM1}} = (+2 J_1) \times N^2/4 + \text{constant (this is AFM5 or AFM4 model in [51], since weaker interactions are omitted)}$$

$$E_{\text{AFM2}} = (+2 J_1 - 2 J_2) \times N^2/4 + \text{constant (this is AFM2 or AFM3 model in [51], since weaker interactions are omitted)}$$

$$E_{\text{FM}} = (-2 J_1 - 2 J_2) \times N^2/4 + \text{constant (this is FM model in [51], since weaker interactions are omitted)}$$

where N is the number of unpaired spins per spin site (in the present case, $N = 1$), one may derive $J_1 = -12$ meV and $J_2 = -62$ meV. The respective values for CuCl_2 calculated with $U = 7$ eV for Cu [51], are: $J_1 = +18.4$ meV and $J_2 = -24.5$ meV. Our results indicate that—like for CuCl_2 — $|J_2| > |J_1|$ and the spin-exchange interactions are geometrically frustrated (Figure 9). Interestingly, however, J_1 is antiferromagnetic for AgCl_2 while ferromagnetic for CuCl_2 . This result probably stems from the fact that antiferromagnetic next neighbor ordering implies null magnetic moments on bridging two Cl atoms, while the FM one introduces very large moments on chloride bridges (Table 3). The former is preferred, as elements which are typical nonmetals (here, in the form of a formally a closed shell Cl^- anion) do not support spin density on them, since it implies breaking of the stable electronic octet. Indeed, the spin density calculated for AgCl_2 in ribbon form suggests that spin density on one type of Cl atoms is as large as $2/3$ of that on silver sites. While this could be expected based on previous studies of Ag(II) in chloride host lattices [52], this factor certainly contributes to lack of stability of AgCl_2 . After all, if most spin sits on Cl atoms, Cl radical tend to pair up and eliminate Cl_2 molecules. This is indeed what one sees when comparing the energy of polymorphic forms of AgCl_2 with respect to phase separated $\text{AgCl} + \frac{1}{2} \text{Cl}_2$. The situation found for CuCl_2 is much different, where the total magnetic moment of circa $0.5\mu_B$ sits mostly on copper site [51].

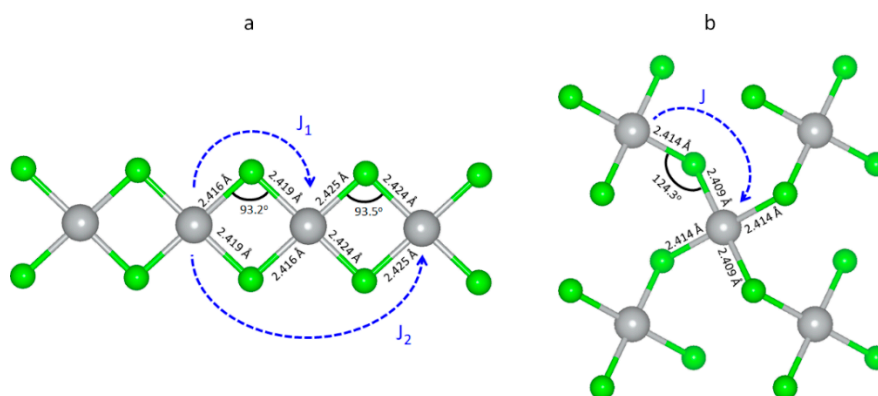


Figure 9. Fragment of the AgCl_2 ribbon with two relevant intra-chain superexchange constants considered in this study (a). Fragment of the corrugated AgCl_2 sheet with one relevant intra-sheet superexchange constant considered here (b).

Let us now scrutinize the magnetic interactions in the layered AgCl_2 polymorph (Table 3, Figure 9).

Here, four identical superexchange pathways link each Ag(II) site to its neighbors, as characterized by intra-sheet superexchange constant, J (the much weaker inter-sheet one will be omitted here). The ground state magnetic model corresponds to the familiar two-dimensional (2D) AFM ordering of spins, assumed also by AgF_2 . Consequently, a spin flip to the FM state costs $(-4J) \times N^2/4$, where $N = 1$. From the energy difference between the AFM and FM solutions we may extract $J = -76$ meV. For comparison the J found for AgF_2 at ambient conditions is -70 meV [53]. This implies a somewhat stronger magnetic superexchange for the Ag–Cl–Ag bridges than for the Ag–F–Ag ones, as indeed could be anticipated from the increased covalence of chemical bonding ($\text{Ag–Cl} > \text{Ag–F}$). This effect is, however, partially diminished by the Ag–Cl–Ag bridges being more bent (124 deg) than their Ag–F–Ag analogues found for AgF_2 (130 deg), and that decreases J for the former system [54], according to the Goodenough-Kanamori rules [55]. Corrugation of the sheets and departure of the Ag–Cl–Ag angle from 180 deg also results in the appearance of the magnetic moment of circa $0.1\mu_B$ at Cl atoms. This is half of what is found for the ribbon polymorph, yet still substantial, and must be viewed as a factor which contributes to the lack of stability of AgCl_2 with respect to elimination of Cl_2 .

3.6. Electronic Properties of Selected Polymorphic Forms of AgCl_2

Having looked at magnetic properties, let us now examine electronic Density of States (DOS) and atomic (partial) DOS for four distinct polymorphs of AgCl_2 (Figure 10).

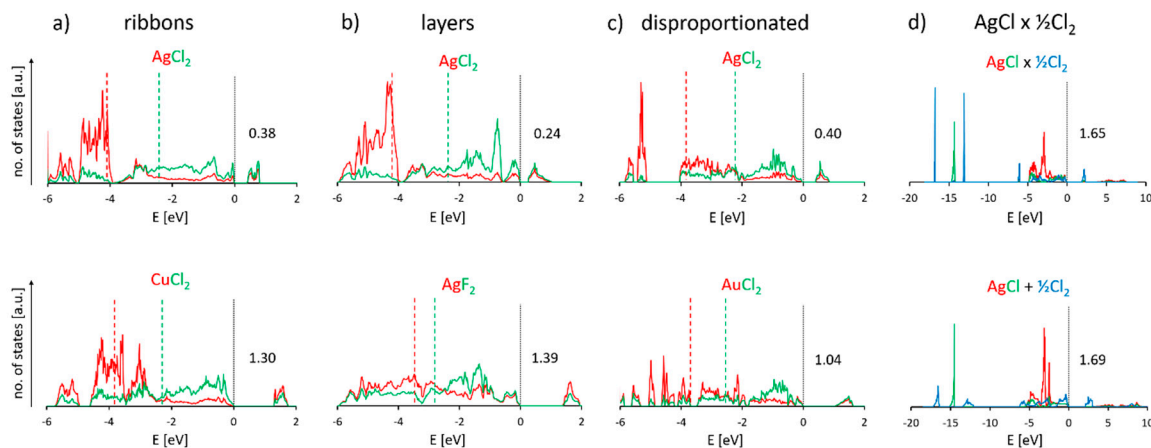


Figure 10. Comparison of the electronic density of states (DOS) graphs of four studied structures of AgCl_2 and their counterparts: (a) ribbon structure and CuCl_2 , (b) layered structure and AgF_2 , (c) disproportionated structure and AuCl_2 , (d) $\text{Ag(I)[Cl(Cl}_2)_{\frac{1}{2}}]$ form with hexagonal AgCl layers and the sum of eDOS of rocksalt AgCl and solid Cl_2 . Red and green dashed lines indicate the DOS-weighted average position of Cu/Ag/Au d and Cl/F p bands, respectively. The number above Fermi level in each graph indicates the fundamental band gap.

A glance at DOS graphs shows that all predicted polymorphs of AgCl_2 were found to have an insulating band gap. However, the calculated band gap at Fermi level tends to be substantially narrower in studied polymorphs of AgCl_2 than in their structural prototypes containing either a different group 11 metal (CuCl_2 , AuCl_2) or a different halogen (AgF_2). In the case of CuCl_2 -like ribbon structure, Ag 4d bands lie comparatively lower in energy than Cu 3d bands and are further separated from occupied Cl 2p states, which is in agreement with the stronger oxidizing properties of Ag(II) species as compared to Cu(II) . The picture is somewhat similar in the layered structure: again, the Ag 4d states in AgCl_2 lie at higher binding energies and are more separated from Cl 2p states than in AgF_2 , where the admixing between Ag 4d and F 1p states in AgF_2 is already substantial [53]. The same applies to the disproportionated form of AgCl_2 (i.e., an AuCl_2 polytype) as compared to its gold(II) analogue. The fact that Ag states are placed deeply below the Cl ones clearly contributes to the lack of stability of AgCl_2 in all polytypes, as oxidation of Cl^- anions by Ag(II) (or Ag(III) in disproportionated form) is facile. This is also reflected in very narrow fundamental bandgaps, which range between a mere 0.24 eV and 0.40 eV. The Maximum Hardness Principle (from Pearson [56]) dictates the preference for much larger bandgap calculated for $\text{AgCl} + \frac{1}{2}(\text{Cl}_2)$ (1.69 eV) and thus to a redox reaction.

As for the AgCl_2 polymorph consisting of hexagonal double layers of AgCl interspersed with layers of Cl_2 molecules, we compared its electronic structure with the combination of eDOS of rocksalt-type AgCl and solid chlorine (HT polymorph). Contributions from in-layer Cl atoms and from Cl_2 molecules between layers in this AgCl_2 polymorph are also plotted separately. The most apparent difference between otherwise similar graphs is that the bands pertaining to Cl_2 molecules are much sharper in AgCl_2 than in solid Cl_2 , which indicates that there is relatively little bonding between them and AgCl layers. On the other hand, Ag 4d bands in AgCl layers of AgCl_2 are somewhat more diffuse than in rocksalt AgCl , which points to a slightly different (more covalent) Ag-Cl bonding character in hexagonal $[\text{AgCl}]$ sublattice of AgCl_2 (as discussed in structural section above) than in ionic AgCl . In addition, the average position of Ag 4d band in this polymorph is circa -3 eV, which is 0.5–1.0 eV higher than in the other three studied polymorphs; this obviously stems from the fact that Ag(I) is present here rather than Ag(II) . In this case, the gap is formed between top of the hybridized $\text{Ag}^+(\text{d})/\text{Cl}^-(\text{p})$ states and the σ^* states of the Cl_2 molecules.

As to the relatively most stable forms of AgCl_2 , i.e., a ribbon and layered polymorph, their band gaps have charge-transfer character; however, in idealized charge-transfer magnetic insulator the gap is formed between occupied nonmetal states (valence band) and the upper Hubbard band on metal

(conduction band). Here, there is so severe mixture of the Ag and Cl states, that the top of the “ligand” band is composed in about 1/3 from Ag states, while the conduction band from a nearly equal mixture of the Ag and Cl states.

4. Conclusions

Our theoretical study for AgCl₂ including outcome of evolutionary algorithm structure prediction method suggests that AgCl₂ is metastable with respect to AgCl + $\frac{1}{2}$ Cl₂ at $p \rightarrow 0$ atm and $T \rightarrow 0$ K conditions. Still, the energy penalty which must be paid for its synthesis from these substrates is relatively small and of the order of 0.1–0.15 eV per formula unit. Thermodynamic stability is smaller at ambient (p,T) conditions and of the order of 0.4 eV per formula unit, due to entropy factor for Cl₂ gas (reaction product). Still, AgCl₂ is not as severely unstable as previously predicted by Morris [2]. If prepared using some non-equilibrium methods, AgCl₂ would be metastable as indicated by lack of imaginary phonon modes for the structures we have scrutinized. AgCl₂ constitutes a challenge for theoretical methods as it allows for diverse charge instabilities, as well as on the verge of decomposition to simpler phases. The most stable polymorphic form of AgCl₂, according to hybrid DFT (HSE06) calculations, is related to CuCl₂ type, and it consists of infinite [AgCl_{4/2}] ribbons. The lowest energy magnetic pattern for this phase is of the AABB type, thus similar to the one shown by CuCl₂. More complex magnetic ordering, i.e., helical, is also possible, due to frustration of NN and NNN superexchange interactions.

Formation of AgCl₂ should be facilitated by use of external pressure, as indicated by extrapolation based on the common tangent method. The thermodynamically stable form at circa 35 GPa has crystal structure related to that of AgF₂; and, like AgF₂, it shows 2D AFM ordering in its ground state.

Having uncovered the chemical identity of the most stable form of AgCl₂ together with its presumed magnetic properties, we may construct a simple table which demonstrates huge difference between coinage group metals [55,57] in terms of their real and hypothetical difluorides and dichlorides (Table 4). Thus, copper, silver, and gold are all different; indeed, the coinage metal group has been argued to contain the most dissimilar elements among all groups of the Periodic Table [58] and this is confirmed in our study of their dichlorides.

Table 4. Comparison of essential features (stability, structure) and magnetic properties (wherever applicable) of Group 11 difluorides and dichlorides, as seen from experiment and theoretical calculations.

Metal	Cu	Ag	Au
MF ₂	Stable Layered 2D AFM [47]	Stable Layered 2D AFM [53]	Unstable Phase separation
MCl ₂	Stable Ribbon 1D complex [51]	Metastable Phase separation [this work]	Stable Disproportionated Diamagnetic [12]

In conclusion, if prepared, AgCl₂ would be a very unusual metastable narrow-band gap (<0.4 eV) magnetic semiconductor. Quest for AgCl₂ should preferably utilize non-equilibrium, high-pressure, and low-T conditions. In the forthcoming work we will report our own attempts toward synthesis of AgCl₂ utilizing the diamond anvil cell setup.

Supplementary Materials: The following are available online at <http://www.mdpi.com/2073-4352/9/8/423/s1>, S1: Analysis of halogen-halogen interactions, S2: list of cif files.

Author Contributions: Conceptualization, W.G. and M.D.; methodology, M.D.; investigation, P.K., K.T. and A.G.; resources, W.G.; data curation, M.D.; writing—original draft preparation, M.D. and W.G.; writing—review and editing, M.D. and W.G.; visualization, M.D.; supervision, M.D. and W.G.; project administration, M.D. and W.G.; funding acquisition, M.D. and W.G.

Funding: Preliminary studies conducted a decade ago were performed within the TEAM project of the Foundation of Polish Science. Subsequent careful scrutiny was possible due to funding from the Polish National Science Center via Maestro project (UMO-2017/26/A/ST5/00570). AG's contribution was financed from Preludium project from NCN (2017/25/N/ST5/01976). MD and KT also acknowledge the Scientific Grant Agency of the Slovak Republic, grant No. VG 1/0223/19.

Acknowledgments: Most calculations were performed at the Interdisciplinary Center for Mathematical and Computational Modelling, the University of Warsaw, at Okeanos machine, within the project ADVANCE++ (GA76-19). MD and KT thank the Centre of operations of the Slovak Academy of Sciences for providing computational resources (supercomputer Aurel) within computation grant "Novel inorganic compounds from ab initio".

Conflicts of Interest: The authors declare no conflict of interest.

References

1. Fajans, K. Electronic Structure of Some Molecules and Crystals. *Ceramic Age* **1949**, *54*, 288.
2. Morris, D.F.C. The instability of some dihalides of copper and silver. *J. Phys. Chem. Solids* **1958**, *7*, 214–217. [[CrossRef](#)]
3. Rossini, F.D.; Wagman, D.D.; Evans, W.H.; Levine, S.; Jaffe, I. Selected values of chemical thermodynamic properties. Circular of National Bureau of Standards No. 500. 1952. Available online: <https://archive.org/details/circularofbureau500ross/page/n7> (accessed on 14 August 2019).
4. Scatturin, V.; Bellon, P.L.; Zannetti, R. Planar coordination of the group IB elements: Crystal structure of Ag (II) oxide. *J. Inorg. Nucl. Chem.* **1958**, *8*, 462–467. [[CrossRef](#)]
5. Yvon, K.; Bezingue, A.; Tissot, P.; Fischer, P. Structure and magnetic properties of tetragonal silver(I, III) oxide, AgO. *J. Solid State Chem.* **1986**, *65*, 225–230. [[CrossRef](#)]
6. Hermann, A.; Derzsi, M.; Grochala, W.; Hoffmann, R. AuO: Evolving from dis- to comproportionation and back again. *Inorg. Chem.* **2016**, *55*, 1278–1286. [[CrossRef](#)] [[PubMed](#)]
7. Gammons, C.H.; Yu, Y.; Williams-Jones, A.E. The disproportionation of gold(I) chloride complexes at 25 to 200 C. *Geochim. Cosmochim. Acta* **1997**, *61*, 1971–1983. [[CrossRef](#)]
8. Malinowski, P.J.; Derzsi, M.; Gawel, B.; Lasocha, W.; Jagličić, Z.; Mazej, Z.; Grochala, W. Ag^{II}SO₄: A Genuine Sulfate of Divalent Silver with Anomalously Strong One-Dimensional Antiferromagnetic Interactions. *Angew. Chem. Int. Ed. Engl.* **2010**, *49*, 1683–1686. [[CrossRef](#)] [[PubMed](#)]
9. Elder, S.H.; Lucier, G.M.; Hollander, F.J.; Bartlett, N. Synthesis of Au(II) fluoro complexes and their structural and magnetic properties. *J. Am. Chem. Soc.* **1997**, *119*, 1020–1026. [[CrossRef](#)]
10. Derzsi, M.; Piekarz, P.; Grochala, W. Structures of late transition metal monoxides from Jahn-Teller instabilities in the rock salt lattice. *Phys. Rev. Lett.* **2014**, *113*, 025505. [[CrossRef](#)]
11. Grzelak, A.; Gawraczyński, J.; Jaroń, T.; Sommayazulu, M.; Derzsi, M.; Struzhkin, V.V.; Grochala, W. Persistence of Mixed and Non-intermediate Valence in the High-Pressure Structure of Silver(I,III) Oxide, AgO: A Combined Raman, X-ray Diffraction (XRD), and Density Functional Theory (DFT) Study. *Inorg. Chem.* **2017**, *56*, 5804–5812. [[CrossRef](#)]
12. Dell'amico, D.B.; Calderazzo, F.; Marchetti, F.; Merlino, S. Synthesis and molecular structure of [Au₄Cl₈], and the isolation of [Pt(CO)Cl₅][−] in thionyl chloride. *J. Chem. Soc., Dalton Trans.: Inorg. Chem.* **1982**, 2257–2260. [[CrossRef](#)]
13. Brückner, R.; Haller, H.; Steinhauer, S.; Müller, C.; Riedel, S. A 2D Polychloride Network Held Together by Halogen–Halogen Interactions. *Angew. Chem. Int. Ed. Engl.* **2015**, *54*, 15579–15583. [[CrossRef](#)] [[PubMed](#)]
14. Taraba, J.; Zak, Z. Diphenyldichlorophosphonium Trichloride–Chlorine Solvate 1:1, [PPh₂Cl₂]⁺Cl₃[−]Cl₂: An Ionic Form of Diphenyltrichlorophosphorane. Crystal Structures of [PPh₂Cl₂]⁺Cl₃[−]Cl₂ and [(PPh₂Cl₂)⁺]₂[InCl₅]^{2−}. *Inorg. Chem.* **2003**, *42*, 3591–3594. [[CrossRef](#)] [[PubMed](#)]
15. Wickleder, M.S. AuSO₄: A True Gold(II) Sulfate with an Au₂⁴⁺ Ion. *Z. Anorg. Allg. Chem.* **2001**, *627*, 2112–2114. [[CrossRef](#)]
16. Derzsi, M.; Dymkowski, K.; Grochala, W. The Theoretical Quest for Sulfate of Ag²⁺: Genuine Ag(II)SO₄, Diamagnetic Ag(I)₂S₂O₈, or Rather Mixed-Valence Ag(I)[Ag(III)(SO₄)₂]? *Inorg. Chem.* **2010**, *49*, 2735–2742. [[CrossRef](#)] [[PubMed](#)]
17. Kurzydłowski, D.; Grochala, W. Elusive AuF in the solid state as accessed via high pressure comproportionation. *Chem. Commun.* **2008**, 1073–1075. [[CrossRef](#)] [[PubMed](#)]

18. Kresse, G.; Hafner, J. Ab initio molecular dynamics for liquid metals. *Phys. Rev. B: Condens. Matter Mater. Phys.* **1993**, *47*, 558–561. [[CrossRef](#)] [[PubMed](#)]
19. Kresse, G.; Hafner, J. Ab initio molecular-dynamics simulation of the liquid-metal–amorphous-semiconductor transition in germanium. *Phys. Rev. B: Condens. Matter Mater. Phys.* **1994**, *49*, 14251–14269. [[CrossRef](#)]
20. Kresse, G.; Furthmüller, J. Efficiency of ab-initio total energy calculations for metals and semiconductors using a plane-wave basis set. *Comput. Mater. Sci.* **1996**, *6*, 15–50. [[CrossRef](#)]
21. Kresse, G.; Furthmüller, J. Efficient iterative schemes for ab initio total-energy calculations using a plane-wave basis set. *Phys. Rev. B: Condens. Matter Mater. Phys.* **1996**, *54*, 11169–11186. [[CrossRef](#)]
22. Kresse, G.; Joubert, D. From ultrasoft pseudopotentials to the projector augmented-wave method. *Phys. Rev. B: Condens. Matter Mater. Phys.* **1999**, *59*, 1758–1775. [[CrossRef](#)]
23. Parlinski, K. *PHONON Software*. 2010. Available online: <http://wolf.ifj.edu.pl/phonon/> (accessed on 2 January 2008).
24. Zurek, E.; Grochala, W. Predicting crystal structures and properties of matter under extreme conditions via quantum mechanics: The pressure is on. *Phys. Chem. Chem. Phys.* **2015**, *17*, 2917–2934. [[CrossRef](#)] [[PubMed](#)]
25. Lonie, D.C.; Zurek, E. XtalOpt: An open-source evolutionary algorithm for crystal structure prediction. *Comput. Phys. Commun.* **2011**, *182*, 372–387. [[CrossRef](#)]
26. Zurek, E.; Hoffmann, R.; Ashcroft, N.W.; Oganov, A.; Lyakhov, A.O. A little bit of lithium does a lot for hydrogen. *Proc. Nat. Acad. Sci. USA* **2009**, *106*, 17640–17643. [[CrossRef](#)] [[PubMed](#)]
27. Baettig, P.; Zurek, E. Pressure-Stabilized Sodium Polyhydrides: NaH_n (n > 1). *Phys. Rev. Lett.* **2011**, *106*, 237002. [[CrossRef](#)]
28. Hooper, J.; Zurek, E. Rubidium Polyhydrides Under Pressure: Emergence of the Linear H₃[−] Species. *Chem. Eur. J.* **2012**, *18*, 5013–5021. [[CrossRef](#)]
29. Liechtenstein, A.I.; Anisimov, V.I.; Zaane, J. Density-functional theory and strong interactions: Orbital ordering in Mott-Hubbard insulators. *Phys. Rev. B* **1995**, *52*, R5467. [[CrossRef](#)]
30. Kasinathan, D.; Kyker, A.B.; Singh, D.J. Origin of ferromagnetism in Cs₂AgF₄: The importance of Ag–F covalency. *Phys. Rev. B* **2006**, *73*, 214420. [[CrossRef](#)]
31. Grimme, S.; Antony, J.; Ehrlich, S.; Krieg, S. A consistent and accurate ab initio parametrization of density functional dispersion correction (DFT-D) for the 94 elements H–Pu. *J. Chem. Phys.* **2010**, *132*, 154104. [[CrossRef](#)]
32. Grochala, W.; Hoffmann, R. Real and Hypothetical Intermediate-Valence Ag^{II}/Ag^{III} and Ag^{II}/Ag^I Fluoride Systems as Potential Superconductors. *Angew. Chem. Int. Ed. Engl.* **2001**, *40*, 2742–2781. [[CrossRef](#)]
33. Grzelak, A.; Gawraczyński, J.; Jaroń, T.; Kurzydłowski, D.; Mazej, Z.; Leszczyński, P.J.; Prakapenka, V.B.; Derzsi, M.; Struzhkin, V.V.; Grochala, W. Metal fluoride nanotubes featuring square-planar building blocks in a high-pressure polymorph of AgF₂. *Dalton Trans.* **2017**, *46*, 14742–14745. [[CrossRef](#)] [[PubMed](#)]
34. Park, S.; Choi, Y.J.; Zhang, C.L.; Cheong, S.W. Ferroelectricity in an S = ½ Chain Cuprate. *Phys. Rev. Lett.* **2007**, *98*, 057601. [[CrossRef](#)] [[PubMed](#)]
35. Gibson, B.J.; Kremer, R.K.; Prokofiev, A.V.; Assmus, W.; McIntyre, G.J. Incommensurate antiferromagnetic order in the S = 12 quantum chain compound LiCuVO₄. *Physica B* **2004**, *350*, e253. [[CrossRef](#)]
36. Yahia, H.B.; Shikano, M.; Tabuchi, M.; Kobayashi, H.; Avdeev, M.; Tan, T.T.; Liu, S.; Ling, C.D. Synthesis and characterization of the crystal and magnetic structures and properties of the hydroxyfluorides Fe(OH)F and Co(OH)F. *Inorg. Chem.* **2014**, *53*, 365–374. [[CrossRef](#)] [[PubMed](#)]
37. Hill, L.I.; Verbaere, A. On the structural defects in synthetic γ-MnO₂s. *J. Solid State Chem.* **2004**, *177*, 4706–4723. [[CrossRef](#)]
38. Evers, J.; Beck, W.; Göbel, M.; Jakob, S.; Mayer, P.; Oehlinger, G.; Rotter, M.; Klapötke, T. The Structures of δ-PdCl₂ and γ-PdCl₂: Phases with Negative Thermal Expansion in One Direction. *Angew. Chem. Int. Ed. Engl.* **2010**, *49*, 5677–5682. [[CrossRef](#)] [[PubMed](#)]
39. Brückner, R.; Haller, H.; Ellwanger, M.; Riedel, S. Polychloride Monoanions from [Cl₃][−] to [Cl₉][−]: A Raman Spectroscopic and Quantum Chemical Investigation. *Chem. Eur. J.* **2012**, *18*, 5741–5747. [[CrossRef](#)]
40. Riedel, E.F.; Willett, R.D. NQR study of the trichloride ion. Evidence for three-center four-electron bonding. *J. Am. Chem. Soc.* **1975**, *97*, 701–704. [[CrossRef](#)]
41. Redeker, F.A.; Beckers, H.; Riedel, S. Matrix-isolation and comparative far-IR investigation of free linear [Cl₃][−] and a series of alkali trichlorides. *Chem. Commun.* **2017**, *53*, 12958–12961. [[CrossRef](#)]

42. Hull, S.; Keen, D.A. Pressure-induced phase transitions in AgCl, AgBr, and AgI. *Phys. Rev. B* **1999**, *59*, 750–761. [[CrossRef](#)]
43. Donohue, J.; Goodman, S.H. Interatomic distances in solid chlorine. *Acta Cryst.* **1965**, *18*, 568–569. [[CrossRef](#)]
44. Jenkins, H.D.B.; Glasser, L. Volume-based thermodynamics: Estimations for 2:2 salts. *Inorg. Chem.* **2006**, *45*, 1754–1756. [[CrossRef](#)] [[PubMed](#)]
45. NIST. gov chemistry webbook database 2019. Available online: <https://webbook.nist.gov/chemistry/> (accessed on 2 July 2019).
46. Horvath-Bordon, E.; Riedel, R.; Zerr, A.; McMillan, P.F.; Auffermann, G.; Prots, Y.; Bronger, W.; Kniep, R.; Kroll, P. High-pressure chemistry of nitride-based materials. *Chem. Soc. Rev.* **2006**, *35*, 987–1014. [[CrossRef](#)] [[PubMed](#)]
47. Kurzydłowski, D. The Jahn-Teller distortion at high pressure: The case of copper difluoride. *Crystals* **2018**, *8*, 140.
48. López-Moreno, S.; Romero, A.H.; Mejía-López, J.; Muñoz, A. First-principles study of pressure-induced structural phase transitions in MnF₂. *Phys. Chem. Chem. Phys.* **2016**, *18*, 33250–33263. [[CrossRef](#)] [[PubMed](#)]
49. Kurzydłowski, D.; Grochala, W. Prediction of extremely strong antiferromagnetic superexchange in silver (II) fluorides: Challenging the oxocuprates (II). *Angew. Chem. Int. Ed. Engl.* **2017**, *56*, 10114–10117. [[CrossRef](#)]
50. Kurzydłowski, D.; Grochala, W. Large exchange anisotropy in quasi-one-dimensional spin- $\frac{1}{2}$ fluoride antiferromagnets with a $d(z^2)^1$ ground state. *Phys. Rev. B* **2017**, *96*, 155140. [[CrossRef](#)]
51. Banks, M.G.; Kremer, R.K.; Hoch, C.; Simon, A.; Ouladdiaf, B.; Broto, J.-M.; Rakoto, H.; Lee, C.; Whangbo, M.-H. Magnetic ordering in the frustrated Heisenberg chain system cupric chloride CuCl₂. *Phys. Rev. B* **2009**, *80*, 024404. [[CrossRef](#)]
52. Aramburu, J.A.; Moreno, M. Bonding of Ag²⁺ in KCl lattice. *Solid State Commun.* **1986**, *58*, 305–309. [[CrossRef](#)]
53. Gawraczyński, J.; Kurzydłowski, D.; Ewings, R.A.; Bandaru, S.; Gadomski, W.; Mazej, Z.; Ruani, G.; Bergenti, I.; Jaroń, T.; Ozarowski, A.; et al. Silver route to cuprate analogs. *Proc. Nat. Acad. Sci. USA* **2019**, *116*, 1495–1500. [[CrossRef](#)]
54. Kurzydłowski, D.; Derzsi, M.; Barone, P.; Grzelak, A.; Struzhkin, V.V.; Lorenzana, J.; Grochala, W. Dramatic enhancement of spin–spin coupling and quenching of magnetic dimensionality in compressed silver difluoride. *Chem. Commun.* **2018**, *54*, 10252–10255. [[CrossRef](#)] [[PubMed](#)]
55. Pyykkö, P. Theoretical chemistry of gold. *Chem. Soc. Rev.* **2008**, *37*, 1967–1997. [[CrossRef](#)] [[PubMed](#)]
56. Pearson, R.G. Recent advances in the concept of hard and soft acids and bases. *J. Chem. Educ.* **1987**, *64*, 561–567. [[CrossRef](#)]
57. Schwerdtfeger, P. Relativistic effects in properties of gold. *Heteroatom Chem.* **2002**, *13*, 578–584. [[CrossRef](#)]
58. Grochala, W.; Mazej, Z. Unique silver (II) fluorides: The emerging electronic and magnetic materials. *Phil. Trans. A* **2015**, *373*, 20140179. [[CrossRef](#)] [[PubMed](#)]

